Observations of ultra-long period normal modes from the 2004 Sumatra-Andaman earthquake

Emile A. Okal and Seth Stein
Department of Earth and Planetary Sciences
Northwestern University, Evanston IL 60208 USA

Physics of the Earth & Planetary Interiors,
Submitted, 26 April 2007

ABSTRACT

The great December 2004 Sumatra-Andaman earthquake was the first "giant" or "extreme" (moment magnitude $M_w \geq 9$) earthquake recorded by broadband digital seismometers whose data were rapidly available to investigators worldwide. As a result, analysis of the earth's longest period normal modes became a primary tool for studying the earthquake, rather than an elegant afterthought. The mode data provided the first evidence that the earthquake was much larger ($M_w \approx 9.3$) than initially inferred from surface wave data and involved slip on a much longer fault than initially inferred from body wave data. These observations in turn yielded important insight into the likely recurrence of similar earthquakes and the resulting tsunamis both on the segment of the trench that ruptured and on neighboring segments. The normal mode data are more numerous and much higher quality than previously available. They thus provide the first direct evidence for effects that had been theoretically predicted, such as the control of the splitting pattern by receiver latitude and the splitting of torsional modes. They similarly yield better results for mode properties such as the attenuation of the longest period radial modes.

INTRODUCTION

Seismological advances often involve three factors. First, a suitable earthquake must generate a signal of interest. Second, the resulting signal must be recorded by appropriate seismometers. Third, the theoretical framework needed to interpret the signal needs to be available.

Studies of the earth's normal modes followed this pattern (Figure 1). *Benioff* [1958] and *Båth* [1958] had hinted that ultra-long period oscillations observed in the time domain following the 1952 Kamchatka and the [much smaller] 1958 Fairweather, Alaska earthquakes might have represented free oscillations of the Earth. However, the undisputed observation and cataloguing of the planet's normal modes, including the gravest, ${}_0S_2$ (T = 3232 s), had to wait until the great 1960 Chilean earthquake [*Alsop et al.,* 1961; *Benioff et al.,* 1961; *Ness et al.,* 1961]. By then, improved

strainmeters and gravimeters had been developed that could record ground motions with periods much longer than possible with existing seismometers, while progress in analytical techniques made it feasible to obtain reliable measurements directly in the frequency domain. In this respect, the 1960 Chilean event had perfect timing. By the time of the great "Good Friday" Alaskan earthquake of 28 March 1964, the newly deployed WWSSN seismometers provided normal mode data at periods of several hundred seconds [*Dziewonski and Gilbert,* 1972], although they were not specifically designed for this application.

By contrast, no truly great earthquake ($M_0 > 10^{29}$ dyn*cm) occurred for nearly 40 years after the 1965 Rat Island event (Figure 1), a time window corresponding grossly to one human generation. This period witnessed several technological revolutions pertinent to seismological research: the acceptance of Plate Tectonics, the explosion of information technology, and the development and generalization of networks of long-period digital instruments, such as the IDA gravimeter network [*Agnew et al.,* 1976] and later the broad-band GEOSCOPE and IRIS Global Seismographic Networks. In this respect, the 2004 Sumatra-Andaman earthquake finally offers a long-overdue combination of the three necessary ingredients for advances in seismological research, especially in the field of the Earth's free oscillations.

THEORETICAL BACKGROUND

With the development of analytical theory and tools [*e.g., Alterman et al.,* 1959], the observation of the Earth's modes in 1960 opened the way for their use in long period studies of earthquake sources and earth structure. These two effects are naturally separated in the normal mode formulation. In *Saito's* [1967] notation using spherical coordinates with the earthquake at the pole, the three-dimensional seismic displacement field $\mathbf{u}(r, \theta, \phi)$ is expanded as a sum of normal modes described by radial order n, angular order l, and azimuthal order m. For spheroidal normal modes, which involve radial (vertical) and transverse motions of the earth analogous to P-SV or Rayleigh waves,

$$\mathbf{u}^S(r, \theta, \phi) = \tag{1}$$

$$= (u_r, u_\theta, u_\phi) = \sum_n \sum_l \sum_{m=-l}^{l} {}_nA_l^m \left[{}_nU_l(r)\, \mathbf{R}_l^m(\theta, \phi) + {}_nV_l(r)\, \mathbf{S}_l^m(\theta, \phi) \right] e^{i\, {}_n\omega_l^m t}\, e^{-\frac{{}_n\omega_l^m t}{2\, {}_nQ_l^m}} ,$$

involving combinations of the spherical harmonics $Y_l^m(\theta, \phi)$

$$\mathbf{R}_l^m = (Y_l^m, 0, 0) \tag{2}$$

$$\mathbf{S}_l^m = \left(0,\ \frac{\partial Y_l^m(\theta,\ \phi)}{\partial \theta},\ \frac{1}{\sin\theta}\ \frac{\partial Y_l^m(\theta,\ \phi)}{\partial \phi}\right)$$

weighted by radial eigenfunctions ${}_nU_l(r)$ for vertical motion and ${}_nV_l(r)$ for horizontal motion.

Similarly, for torsional normal modes, which involve horizontal motions of the earth analogous to *SH* or Love waves, the displacement vector is written

$$\mathbf{u}^T(r,\ \theta,\ \phi) = \sum_n \sum_l \sum_{m=-l}^{l} {}_nB_l^m\ {}_nW_l(r)\ \ \mathbf{T}_l^m(\theta,\ \phi)\ e^{i\ {}_n\omega_l^m t}\ e^{-\frac{{}_n\omega_l^m t}{2\ {}_nQ_l^m}}. \tag{3}$$

where

$$\mathbf{T}_l^m = \left(0,\ \frac{1}{\sin\theta}\ \frac{\partial Y_l^m(\theta,\ \phi)}{\partial \phi},\ \frac{-\partial Y_l^m(\theta,\ \phi)}{\partial \theta}\right). \tag{4}$$

The modes' radial eigenfunctions and eigenfrequencies ${}_n\omega_l^m$ are determined by the earth's velocity and density structure (Alterman et al., 1959). Similarly, the modes' attenuation is expressed through their quality factor ${}_nQ_l^m$, that depends on the distribution of anelasticity in the earth [*Sailor and Dziewonski,* 1978]. (The values of ${}_n\omega_l^m$ and ${}_nQ_l^m$ are different for spheroidal and torsional modes sharing the same indices, but to simplify the notation, we use the same symbols, as the nature of the mode involved is usually evident from the context.) Following an earthquake, the displacement contributed by each mode is determined by its excitation amplitudes ${}_nA_l^m$ or ${}_nB_l^m$, that depend on the depth, geometry, and time history of the seismic source [*Saito,* 1967; *Gilbert,* 1970].

In this context, normal mode data are used for studies of both earth structure, by focusing on ω and Q [*e.g., Gilbert and Dziewonski,* 1975], and earthquake sources by focusing on the parameters A and B [*e.g., Kanamori and Cipar,* 1974]. Such studies are typically termed "normal mode" studies when they consider individual modes, and "surface wave" studies when they treat a set of modes as a continuous spectrum, usually through the use of an asymptotic expansion of the spherical harmonics to express travelling waves [*Kanamori and Stewart,* 1976].

While normal mode studies continued during the age of mega-earthquake quiescence (1965-2004), they had to be confined to smaller, if still "great" ($M_w \geq 8$), earthquakes such as the 1977 Indonesia, 2001 Peru, or deep 1994 Bolivia events. Most studies [*e.g., Buland et al.,* 1979; *Geller and Stein,* 1979; *Riedesel et al.,* 1980; *Stein and Nunn,* 1981; *Widmer et al.,* 1992] focused on measuring eigenfrequencies and attenuation, although some addressed source properties [*e.g., Ekström,* 1995; *Okal,* 1996]. The latter typically were conducted well after the earthquake and focused on refining a source model developed from body and surface wave data.

PREVIOUS RESULTS

The rapid availability of normal mode data following the December 26, 2004 Sumatra-Andaman (or "Sumatra") earthquake led to a new approach. This event was the first $M_w \geq 9$ earthquake since the 1964 Alaskan event. Its enormous size and its devastating tsunami promoted a wide range of studies by earth scientists around the world. These studies were greatly facilitated by the availability in near-real time of high quality seismological, geodetic, and other geophysical data. Information became rapidly available, making this the best studied earthquake of its size, and providing a basis for studies that will likely continue for many years.

Focusing initially on ultra-long period ($T > 500$ s) observations of normal modes from the Global Seismic Network, we showed in *Stein and Okal* [2005] that the earthquake was much larger and involved slip on a much longer fault than at first thought. This analysis, published three months after the earthquake, provided insight into the generation of the tsunami, the recurrence time of similar earthquakes, and the regional tectonics. A key result was that, because the entire aftershock zone slipped, strain accumulated from subduction of India beneath the Burma microplate (or sliver) along the northern part of the rupture had also been released. This left no immediate danger of a similar oceanwide tsunami being generated by slip on that segment of the plate boundary. Because of the complexity of the local tectonic regime (*e.g.,* the northern extent of the Burma sliver is not precisely known), the eventuality of a megathrust earthquake immediately to the north of the 2004 rupture cannot be totally discounted [*Okal and Synolakis,* 2007]. Conversely, we pointed out in *Stein and Okal* [2005] the possibility of a large earthquake on the neighboring trench segment to the south, a scenario described at the same time in greater detail by *McCloskey et al.* [2005], in the framework of Coulomb stress transfer. Such an event, the Simeulue-Nias earthquake ($M_w = 8.7$) occurred on March 28, 2005. Our subsequent studies [*Stein and Okal,* 2007] and those of many other investigators [*e.g., Banerjee et al.,* 2005; *Ishii et al.,* 2005; *Tsai et al.,* 2005; *Ni et al.,* 2005; *Park et al.,* 2005; *Vigny et al.,* 2005] generally supported these initial findings and provided considerably more information.

NORMAL MODE DATA

The longest period normal modes of the Earth are well excited only by the very largest earthquakes which have sufficient energy at long periods, and thus provide information on the longest period portions of the earthquake source.

A simplified approach to the Earth's normal modes treats the planet as an idealized spherically symmetric, non-rotating, purely elastic, and isotropic body. In that case, a mode's angular frequency ${}_n\omega_l^m$ depends only on n and l; in other words, the $2l + 1$ singlets with different azimuthal orders $-l \leq m \leq l$ would have the same eigenfrequency. However, in the real Earth, rotation, ellipticity, and lateral heterogeneity all concur to remove this degeneracy, making the singlet frequencies

slightly dependent on m. This effect, named mode splitting and reaching ±3% in relative frequency for the longest period modes, and was first observed for the 1960 Chilean earthquake [*Pekeris et al.,* 1961; *Backus and Gilbert,* 1961]. Its theory was given by *Dahlen* [1968] and algorithms for the computation of individual eigenfrequencies split by ellipticity and rotation were published by *Dahlen and Sailor* [1979]. *Stein and Geller* [1977] later derived excitation coefficients of the various singlets by seismic sources of arbitrary geometry, under the same conditions, namely accounting for earth's rotation and ellipticity, but not lateral heterogeneity. While these authors applied their formalism to the quantification of records of the 1960 Chilean and 1964 Alaskan earthquakes, painstakingly hand-digitized from analog records [*Stein and Geller,* 1978], no large enough earthquake occurred in the ensuing 25 years to allow the application (or even the systematic verification) of their formalism to very large high-quality datasets. The 2004 Sumatra earthquake constitutes the first such opportunity.

To investigate spheroidal modes, we used 30-day time series of vertical seismograms obtained on the very-long-period channels of the IRIS and GEOSCOPE networks. Stations with inadequate noise level or prolonged gaps in their time series were eliminated. The records were Fourier-analyzed and the instrument response deconvolved to obtain the spectral amplitudes $U(\omega)$, expressed in cm*s. The spectra clearly exhibit split modes, as illustrated in Figure 2 for the seven singlets making up the ${}_0S_3$ multiplet, with an unsplit period of 2135 s. Although the spectral lines of individual singlets are broadened by anelasticity and use of a finite time window, the frequency splitting is large enough that the peaks are distinct, and thus ideal for studies of the earthquake source. The records also showed beautifully split ${}_0S_2$ (3232 s) and ${}_0S_4$ (1545 s) multiplets, whereas the peaks for ${}_0S_5$ (1190 s) and ${}_0S_6$ (964 s) overlap. In addition to these fundamental modes, we targeted for study all spheroidal overtones with period $T > 850$ s, as well as the first radial overtone ${}_1S_0$ ($T = 613$ s). Of those, the only two which could not be resolved were the core mode ${}_2S_2$ (see discussion below), and the elusive Slichter mode ${}_1S_1$ expressing the bobbing of the inner core about the center of the Earth, which remains one the last Holy Grails of observational seismology.

Torsional modes are in general more attenuated than their spheroidal counterparts; as a result, their amplitudes decay faster and their spectral lines are broader. This limited useful time series to 15 days rather than 30, further restricting sampling in the frequency domain and hence our ability to resolve singlets. Nevertheless, the diversity of the broad spectra predicted by *Stein and Geller*'s [1977] splitting formalism is well reproduced by the data. Figure 3 shows the case of the fundamental torsional mode, ${}_0T_2$, which had not been observed prior to the Sumatra earthquake. The best fit to the observed spectrum requires an adjustment of the unperturbed frequency of the mode, increasing its period by approximately 5.5 s, or 0.21%. Similarly, Figure 4 shows a spectrum of the previously unobserved spheroidal mode ${}_2S_1$, identifiable only on horizontal instruments because of the flattened aspect ratio of its displacement eigenfunction at the Earth's surface ($u_x/u_z = 19$). Again,

we propose a red shift of ~ 0.8 μHz or +5 s of the unsplit frequency of the mode.

For each record, we modeled the amplitudes of individual singlets using *Stein and Geller*'s [1977] approach, which maps the excitation of singlets from the frame of reference of the earthquake source into the geographic frame of reference about the north polar axis, by transforming spherical harmonics from one frame into the other. (For torsional modes, we correct the sign of the term p_1 in their Equation (4.9), which should therefore read

$$p_1 = \frac{1}{4} (\sin \lambda \cos 2\delta + i \cos \lambda \cos \delta) \tag{5}$$

all other equations being unchanged.) The use of spherical harmonics in the geographic frame is needed because rotation and ellipticity are symmetric about the Earth's polar axis. Although in the source coordinate frame only singlets with $m = 0, \pm 1, \pm 2$ are excited by a double couple, all $2l + 1$ singlets are excited in the geographic frame. The amplitudes of individual singlets depend on the locations of the earthquake and seismic station, earthquake depth, focal mechanism, and seismic moment.

Our first modeling experiments used a point-source double-couple. Once a source location is chosen, the splitting pattern is controlled by station latitude; we believe that the remarkable dataset in Figure 5 constitutes the first generalized observation of this property. Note in particular the prominence of the central singlet ($m = 0$) at the high latitude station DRV, and of the even singlets ($m = 0, \pm 2$) in the equatorial band (KMB, NNA). Furthermore, for a given station (*e.g.,* OBN; Figure 6), the splitting pattern depends critically on the latitude of the source. For the gravest mode ${}_0S_2$, the approximation of a point-source double-couple can be used to best-fit the observed pattern, and thus define a centroid of the rupture, at a latitude of about 7°N (Figure 6), suggesting that faulting occurred along the entire aftershock zone. This appeared discordant with initial body wave inversions [*e.g., Ji,* 2005] that constrained the rupture to a 300–km segment extending northwards from the epicenter (Figure 6). As discussed below, most later analyses using a large variety of seismological and other techniques later upheld our interpretation.

For a given double-couple geometry, it is possible to derive a source size (expressed as a seismic moment M_0 by best-fitting the observed and synthetic signals, either in the time domain (after narrow band-pass filtering the records) or in the spectral domain as shown on Figure 2. For this purpose, we used the focal mechanism (strike $\phi = 329°$, dip $\delta = 8°$, and slip $\lambda = 110°$) and depth ($h = 28$ km) reported by the Harvard CMT project, and the splitting parameters of individual modes listed by *Dahlen & Sailor* [1979]. The quality of the data is such that several singlets can be filtered out of the records and modeled individually in the time domain, as shown on Figure 7.

SOURCE SPECTRUM

By combining data at different stations for each mode, we obtained a best-fitting value for the seismic moment released at that period, under the assumption of a point-source double-couple. Table 1 lists our results obtained in the frequency domain. These values, summarized in Figure 8*a*, confirm our initial results [*Stein and Okal,* 2005], namely a systematic increase with increasing period of the moment determined from fundamental spheroidal modes, and also extend this effect to spheroidal overtones and torsional modes. In particular, the moment measured for ${}_0S_2$, 1.03×10^{30} dyn*cm (equivalent to $M_w = 9.3$) is approximately 2.5 times larger than the Harvard CMT solution (3.95×10^{29} dyn*cm), even though the latter exceptionally made use of 300–s surface waves (as opposed to the standard 135 s). Whatever the precise value, this is clearly a giant earthquake. As noted by *Stein and Okal* [2007], Figure 8*b* shows that this trend is absent for the 2005 Nias earthquake, which would have been the largest event in 40 years, but for the 2004 Sumatra one.

In order to reconcile estimates of M_0 at various periods, we modeled our dataset using *Tsai et al.*'s [2005] composite CMT source. The latter comprises five point sources offset in time and space along the rupture with varying amplitudes and focal mechanisms (Figure 9*a*). For each of the 370 records used (involving 16 modes), we compute the synthetic spectrum expected from these authors' model, and scale it to our spectra, allowing only the overall moment of the full source to float, all other parameters, including the geometry of the five sources and their relative amplitudes, remaining fixed.

Figure 9*b* shows that our data is best fit using $M_0 = 1.21 \times 10^{30}$ dyn*cm, with an error bar expressed as a multiplicative or divisive factor of 1.12, in excellent agreement with *Tsai et al.*'s [2005] value of 1.18×10^{30} dyn*cm. Note in particular that the "new" overtone and torsional data also fit the pattern, and that this composite solution considerably reduces the scatter between individual stations for such modes as ${}_0T_2$, ${}_1S_2$ and ${}_2S_1$.

The effect of a source spread out in time and space on the excitation of an Earth's mode is perhaps best illustrated in the case of the radial mode ${}_0S_0$, for which excitation is independent of source location. As the individual elements in the composite source are switched "on", they reset the mode out of phase with the oscillation of the previous sources, resulting in destructive interference, a smaller observed spectral amplitude, and hence in an underestimation of the full seismic moment released when modeled as a single point source. The effect is exacerbated for the non-radial modes, for which excitation is also a function of epicentral location.

The fundamental elements of *Tsai et al.*'s [2005] model upheld by our investigation – a large moment of about 10^{30} dyn*cm and a fault length of 1200 km – translate into an average seismic slip $\Delta u \approx 11$ m for a down-dip fault dimension of 200 km. This is also in general agreement with the results of various tomographic source studies based on geodetic data [*Vigny et al.,* 2005; *Banerjee et al.,* 2007]. When allowing for documented scatter about this average, this also fits the observed

maximum tsunami run-up of 32 m in the near field [*Synolakis et al.,* 2007], within a factor of 2 of Δu, as predicted numerically by *Okal and Synolakis* [2004] for elastic dislocations and a regularly shaped local beach. The longer rupture required by the modeling on Figure 6 is also consistent with far-field tsunami observations, since the lobe of maximum directivity, which is always at right angles to the direction of faulting [*Ben-Menahem and Rosenman,* 1972], impacts Sri Lanka and even Somalia, where catastrophic damage was indeed reported [*Fritz and Borrero,* 2006]. In contrast, it would be directed towards Madagascar and the Mascarenes instead, under the shorter fault model assuming slip only on its southern part.

Another important aspect of our results is that the correct modeling of all modes by a common source across a broad frequency spectrum requires a source extending both in time and space as in the model of *Tsai et al.* [2005]. Their composite source is remarkable in that it corresponds to an average propagation velocity of the rupture along the fault zone of 2.8 km/s which is significantly slower than the value of 3 to 3.5 km/s (or roughly 0.8 times the source shear velocity) predicted by seismic scaling laws on the basis of large datasets of rupture velocities obtained from generally smaller earthquakes. While the 2004 Sumatra earthquake does not feature the exceedingly slow ruptures ($V_R \approx 1$ km/s) typical of the so-called "tsunami earthquakes" [*e.g., Polet and Kanamori,* 2000; *López and Okal,* 2006], its relatively slow rupture velocity has been confirmed by many independent studies using totally different techniques [*Ishii et al.,* 2005; *Krüger and Ohrnberger,* 2005; *de Groot-Hedlin,* 2005; *Tolstoy and Bohnenstiehl,* 2005; *Guilbert et al.,* 2005; *Reymond and Okal,* 2006].

In our view, the crucial result from our studies is not the precise value of the moment or moment magnitude, and whether the Sumatra earthquake was the second or third largest earthquake ever recorded. The 2004 event, the most studied large earthquake to date with the best and most diverse data, demonstrates again that such quantities have uncertainties (typically 0.1 to 0.2 units in moment magnitude, or as much as a factor of 2 in moment) owing to the diversity in data type, the specific data used, and to the variety of assumptions required in the analysis. It may be futile to attempt to characterize an event of such documented complexity with a single number, an admittedly appealing goal, but an endeavor known to be doomed ever since it occupied such founding fathers of quantitative seismology as Gutenberg and Richter for several decades in their unsuccessful quest for the "unified" magnitude. Even the seismic moment, a modern physical variable, cannot fully describe an earthquake source of the size and complexity of the 2004 Sumatra event.

Rather, and in the long run, the most important characterization of the truly exceptional size of the 2004 Sumatra earthquake will probably be expressed in the tectonic context, specifically in terms of its contribution to the seismic cycle of that subduction zone, which, regrettably, was totally

misrepresented before 2004, and of which many aspects remain poorly known even in the aftermath of the event.

OTHER ASPECTS: THE Q of RADIAL MODES ${}_0S_0$ and ${}_1S_0$

We conducted a special analysis of the radial modes ${}_0S_0$ and ${}_1S_0$ which contain only one singlet and thus are not split. The oscillations of these so-called "breathing" modes involve mostly changes in material density, but only limited shear. Thus, their anelastic attenuation Q^{-1} is small, and significantly controlled by the Earth's bulk attenuation Q_K^{-1}, whose magnitude remains poorly constrained, as it is substantially smaller than its shear counterpart Q_μ^{-1}. As discussed by *Okal* [1996], the accurate study of the spectral lines of the radial modes requires times series lasting on the order of the product of their period T by their quality factor Q.

In the case of ${}_0S_0$, the exceptional quality of the data allows us to use a window of 85 days at four stations (CTA, MAJO, PPT and YSS), limited in practice only by the occurrence of the Nias event on 28 March 2005. The isotropic character of the radial modes also guarantees that records at various stations are always in phase, regardless of the mechanism and depth of the source, thus optimizing the procedure of stacking. On Figure 10, we process a stack of those four records. After narrow-bandpass filtering between 0.8084 and 0.8224 mHz, we compute a Hilbert-transform envelope, and best-fit a straight line to its logarithm, which yields $Q = 5579 \pm 140$. The remarkable linearity of the logarithmic decay of the mode with time is contrasted on Figure 11 with its counterpart for the 2001 Peruvian earthquake, the largest event prior to 2004 for which digital data of comparable quality was available. Also shown are results for the 2005 Nias earthquake. Figure 11*b* also shows that only the Sumatra measurements are robust with respect to the duration of the processing. In summary, owing to the earthquake's huge size and the newer instrumentation, our estimate is better constrained than the previously published value ($Q = 5700 \pm 256$) [*Riedesel et al.,* 1980], with which it is nevertheless consistent at the $1-\sigma$ confidence level.

The Q of ${}_1S_0$ was similarly estimated at $Q = 2017 \pm 84$ on the basis of nine stacked records of 13−day duration.

THE CASE of ${}_2S_2$

In a recent abstract, *Nishiguchi et al.* [2006] have claimed the observation, on seismic very-broadband instruments, of the previously unreported inner core mode ${}_2S_2$, whose unsplit period (T = 1055 s) is also very close to those of ${}_1S_3$ and ${}_3S_1$. We have explored this issue both theoretically and through modeling of available spectra, and conclude that ${}_2S_2$ could not have been excited above the noise level. Figure 12 uses the spectrum at Black Forest Observatory (BFO) to explore the relative contributions of the three modes. On the left panel, we show that the sharp peaks around

0.945 mHz belong to ${}_3S_1$ (a mode adequately sampling both mantle and core), while the hump around 0.935 mHz represents ${}_1S_3$ (a more strongly attenuated mantle mode whose singlets are poorly separated). The central panel shows that the full spectrum is well modeled by a combination of those two modes. On the other hand, the addition of ${}_2S_2$ (right panel) only produces a minor alteration to the theoretical spectrum, which does not emerge from the residual noise of the fit by the other two modes. This is easily explained since the eigenfunction of ${}_2S_2$ features a displacement primarily confined to the inner core and the bottom third of the outer core. As a result, its excitation coefficients for shallow earthquakes (typically 28 km as used in the present study) are one order of magnitude smaller than those of ${}_1S_3$ and ${}_3S_1$. Although this conclusion was reached by *Nishiguchi et al.* [2006], we observe that the relevant spectral amplitude remains within the noise, especially given the critically short time series which they used (at most 12 hours). Furthermore, we note that *Nishiguchi et al.* [2006] do not consider splitting when directly interpreting power spectrum peaks as multiplets, and thus we question their interpretation, as well as their conclusions regarding shear attenuation in the inner core.

Similarly, *Braitenberg and Zadro* [2007] claim to have detected ${}_2S_2$ on strainmeter records at Trieste. However, these authors' relatively short time series (75 hours) lacks sufficient resolution to separate singlets, forcing them to ignore splitting for all but the very gravest Earth's modes. Thus the exact association of the spectral lines they identify with the individual singlets making up the ${}_1S_3 - {}_3S_1 - {}_2S_2$ combination is questionable.

CONCLUSIONS

The extraordinary quantity and quality of ultra-long period normal mode data from the December 2004 Sumatra-Andaman earthquake provide a powerful tool for investigations of the earthquake source and earth structure. Torsional mode data confirm previous estimates of the earthquake moment inferred from spheroidal data. Radial mode data provide better estimates of their attenuation than previously possible.

The slow source of the 2004 Sumatra earthquake, which owes its documentation at least partially to the study of Earth's gravest normal modes, raises the interesting question of whether all megathrust earthquakes exhibit slowness. This property has long been known for the 1960 Chilean earthquake [*Kanamori and Cipar,* 1974; *Cifuentes and Silver,* 1989], and *Nettles et al.* [2005] have recently proposed revising the moment of the 1964 Alaskan earthquake upwards to as much as 1.3×10^{30} dyn*cm, or about 1.5 times its value obtained from conventional mantle waves [*Kanamori,* 1970]. The present results suggest that the 2004 earthquake follows this trend. By contrast, the 2005 Nias earthquake features the mostly regular source characteristics of an earthquake obeying scaling laws. Unfortunately, in the absence of digital data, it may be impossible to adequately investigate in this respect the crucial runner-ups in terms of size (Kamchatka, 1952;

Aleutian, 1957). Yet, source slowness, as expressed for example by an energy-to-moment ratio [*Boatwright and Choy,* 1986; *Newman and Okal,* 1998] is a fundamental parameter directly related to such socially relevant variables as the relative impact of the shaking and the tsunami on local communities. This was vividly expressed on the horrific videos of the 2004 tsunami flooding the streets of Banda Aceh, between rows of buildings left intact from the shaking by the earthquake, which thus had to have been relatively weak. It is clear that the understanding of deviations from scaling laws in the context of global tectonics, with the ultimate aim of their reliable inclusion in realistic scenarios of future disasters, remains a formidable challenge to the seismological community.

ACKNOWLEDGMENTS

This research was supported in part by the National Science Foundation under grant CMS-03-01054. Several figures were drafted using the GMT package [*Wessel and Smith,* 1991]. We thank Meredith Nettles for access to the Composite Harvard CMT solution before publication.

REFERENCES

Agnew, D., B. Berger, R. Buland, W. Farrell, and F. Gilbert, International deployment of accelerometers: A network for very long period seismology, *Eos, Trans. Amer. Geophys. Un.,* **57,** 180–188, 1976.

Alsop, L. E., G. Sutton, and M. Ewing, Free oscillations of the Earth observed on strain and pendulum seismographs, *J. Geophys. Res.,* **66,** 631–641, 1961.

Alterman, Z. S., H. Jarosch, and C. L. Pekeris, Oscillations of the Earth, *Proc. Roy. Soc. London, Ser. A,* **252,** 80–95, 1959.

Ammon, C. J., C. Ji, H-K. Thio, D. Robinson, S. Ni, V. Hjorleifsdottir, H. Kanamori, T. Lay, S. Das, D. Helmberger, G. Ichinose, J. Polet, and D. Wald, Rupture process of the 2004 Sumatra-Andaman earthquake, *Science,* **308,** 1133–1139, 2005.

Backus, G., and F. Gilbert, The rotational splitting of the free oscillations of the Earth, *Proc. Nat. Acad. Sci. US,* **47,** 362–371, 1961.

Banerjee, P., F. F. Pollitz, and R. Bürgmann, The size and duration of the Sumatra-Andaman earthquake from far-field static offsets, *Science,* **308,** 1769–1772, 2005.

Banerjee, P., F. Pollitz, B. Nagarajan, and R. Bürgmann, Coseismic slip distributions of the 26

December 2004 Sumatra-Andaman and 28 March 2005 Nias earthquakes from GPS static offsets, *Bull. Seismol. Soc. Amer.,* **97,** S86–S102, 2007.

Båth, M., Ultra-long-period motions from the Alaska earthquake of July 10, 1958, *Pure Appl. Geophys.,* **41,** 91–100, 1958.

Benioff, H., Long waves observed in the Kamchatka earthquake of November 4, 1952, *J. Geophys. Res.,* **63,** 589–593, 1958.

Benioff, H., F. Press, and S. Smith, Excitation of the free oscillations of the Earth by earthquakes, *J. Geophys. Res.,* **66,** 605–619, 1961.

Ben-Menahem, A., and M. Rosenman, Amplitude patterns of tsunami waves from submarine earthquakes, *J. Geophys. Res.,* **77,** 3097–3128, 1972.

Boatwright, J., and G.L. Choy, Teleseismic estimates of the energy radiated by shallow earthquakes, *J. Geophys. Res.,* **91,** 2095–2112, 1986.

Braitenberg, C., and M. Zadro, Comparative analysis of free oscillations generated by the Sumatra-Andaman Islands 2004 and the Chile 1960 earthquakes, *Bull. Seismol. Soc. Amer.,* **97,** S6–S17, 2007.

Buland, R., J. Berger, and F. Gilbert, Observations from the IDA network of attenuation and splitting during a recent earthquake, *Nature,* **277,** 358–62, 1979.

Cifuentes I., and P.G. Silver, Low-frequency source characteristics of the great 1960 Chilean earthquake, *J. Geophys. Res.,* **94,** 643–663, 1989.

Dahlen, F.A., The normal modes of a rotating, elliptical Earth, *Geophys. J. Roy. astr. Soc.,* **16,** 329–367, 1968.

Dahlen, F. A., and R. V. Sailor, Rotational and elliptical splitting of the free oscillations of the Earth, *Geophys. J. R. astron. Soc.,* **58,** 609–623, 1979.

de Groot-Hedlin, C.D., Estimation of the rupture length and velocity of the great Sumatra earthquake of Dec. 26, 2004 using hydroacoustic signals, *Geophys. Res. Letts.,* **32,** *(11),* L11303, 4 pp., 2005.

Dziewonski, A.M., and F. Gilbert, Observations of normal modes from 84 recordings of the Alaskan earthquake of 1964 March 28, *Geophys. J. Roy. astr. Soc.,* **27,** 393–446, 1972.

Ekström, G., Static deformation following the Bolivia earthquake by summation of Earth's normal modes, *Geophys. Res. Letts.,* **22,** 2289–2292, 1995.

Fritz, H.M., and J.C. Borrero, Somalia field survey after the December 2004 Indian Ocean tsunami, *Earthquake Spectra,* **22,** S219–S233, 2006.

Geller, R. J., and S. Stein, Time domain attenuation measurements for fundamental spheroidal modes ($_0S_6 - {}_0S_{28}$) for the 1977 Indonesian earthquake, *Bull. Seismol. Soc. Am.,* **69,** 1671–1691, 1979.

Gilbert, F., Excitation of the normal modes of the Earth by earthquake sources, *Geophys. J. R.*

astron. Soc., **22,** 223–226, 1970.

Gilbert, F., and A. M. Dziewonski, An application of normal mode theory to the retrieval of structural parameters and source mechanisms from seismic spectra, *Phil. Trans. R. Soc. Lond., Ser. A,* **278,** 187–269, 1975.

Guilbert, J., J. Vergoz, E. Schisselé, A. Roueff, and Y. Cansi, Use of hydroacoustic and seismic arrays to observe rupture propagation and source extent of the $M_w = 9.0$ Sumatra earthquake, *Geophys. Res. Lett.,* **32,** *(15),* L15310, doi:10.1029/2005GL022966, 4 pp., 2005.

Ishii, M., P. M. Shearer, H. Houston, and J. E. Vidale, extent, duration, and speed of the 2004 Sumatra-Andaman earthquake imaged by the Hi-Net array, *Nature,* **435,** 933–936, 2005.

Ji, C, *http://neic.usgs.gov/neis/eq_depot/2004/eq_041226/neic_slav_ff.html,* 2005.

Kanamori, H., The Alaska earthquake of 1964: Radiation of long-period surface waves and source mechanism, *J. Geophys Res.* **75,** 5029–5040, 1970.

Kanamori, H., and J. J. Cipar, Focal process of the great Chilean earthquake May 22, 1960, *Phys. Earth Planet. Inter.,* **9,** 128–136, 1974.

Kanamori, H., and G. S. Stewart, Mode of the strain release along the Gibbs Fracture Zone, Mid-Atlantic Ridge, *Phys. Earth Planet. Inter.,* **11,** 312–332, 1976.

Krüger F., and M. Ohrnberger, Spatio-temporal source characteristics of the 26 December 2004 Sumatra earthquake as imaged by teleseismic broadband arrays, *Geophys. Res. Letts.,* **32,** *(24),* L24312, 4 pp.,2005.

López, A.M., and E.A. Okal, A seismological reassessment of the source of the 1946 Aleutian "tsunami" earthquake, *Geophys. J. Intl.,* **165,** 835–849, 2006.

McCloskey, J., S.S. Nalbant, and S. Steacey, Earthquake risk from coseismic stress, *Nature,* **434,** 291, 2005.

Nettles, M., G. Ekström, A. Dziewoński, and M. Maternovskaya, Source characteristics of the great Sumatra earthquake and its aftershocks, *Eos, Trans. Amer. Geophys. Un.,* **86,** *(18),* U43A-01, 2005 [abstract].

Ness, N. F., J. C. Harrison, and L. B. Slichter, Observations of the free oscillations of the Earth, *J. Geophys. Res.,* **66,** 621–629, 1961.

Newman, A.V., and E.A. Okal, Teleseismic estimates of radiated seismic energy: The E/M_0 discriminant for tsunami earthquakes, *J. Geophys. Res.,* **103,** 26885–26898, 1998.

Ni, S., H. Kanamori, and D. Helmberger, Energy radiation from the Sumatra earthquake, *Nature,* **434,** 582, 2005.

Nishiguchi, T., I. Kawasaki, and W. Morii, The core mode of ${}_2S_2$ (1055 s) excited by the 2004 great Sumatra-Andaman earthquake, *Japan Geoscience Union meeting, Chiba, Japan,* Abstract I143-001, 2006 [abstract].

Okal, E. A., Radial modes from the great 1994 Bolivian earthquake: no evidence of an isotropic

component to the source, *Geophys. Res. Lett.,* **23,** 431–434, 1996.

Okal, E.A., and C.E. Synolakis, Source discriminants for near–field tsunamis, *Geophys. J. Intl.,* **158,** 899–912, 2004.

Okal, E.A., and C.E. Synolakis, Far-field tsunami risk from mega-thrust earthquakes in the Indian Ocean, *Geophys. J. Intl.,* submitted, 2007.

Park, J., T.-R. A. Song, J. Tromp, E. Okal, S. Stein, G. Roult, E. Clévédé, G. Laske, H. Kanamori, P. Davis, J. Berger, C. Braitenberg, M. van Camp, X. Lei, H. Sun, H. Xu, and S. Rosat, Earth's free oscillations excited by the 26 December 2004 Sumatra-Andaman earthquake,, *Science,* **308,** 1139–1144, 2005.

Pekeris, C. L., Z. Alterman, and H. Jarosch, Rotational multiplets in the spectrum of the Earth, *Phys. Rev.,* **122,** 1692–1700, 1961.

Polet, J., and H. Kanamori, Shallow subduction zone earthquakes and their tsunamigenic potential, *Geophys. J. Intl.,* **142,** 684–702, 2000.

Reymond, D., and E.A. Okal, Rapid, yet robust source estimates for challenging events: Tsunami earthquakes and mega-thrusts, *Eos, Trans. Amer. Geophys. Un.,* **87,** *(52),* S14A-02, 2006 [abstract].

Richter, C. F., An instrumental earthquake magnitude scale, *Bull. Seismol. Soc. Am.,* **25,** 1–32, 1935.

Riedesel, M., D. Agnew, J. Berger, and F. Gilbert, Stacking for the frequencies and Qs of ${}_0S_0$ and ${}_1S_0$, *Geophys. J. Roy. astr. Soc.,* **62,** 457–471, 1980.

Sailor, R. V., and A. M. Dziewonski, Measurements and interpretation of normal mode attenuation, *Geophys. J. R. astron. Soc.,* **53,** 559–581, 1978.

Saito, M., Excitation of free oscillations and surface waves by a point source in a vertically heterogeneous Earth, *J. Geophys. Res.,* **72,** 3689–3699, 1967.

Stein, S., and R. J. Geller, Amplitudes of the split normal modes of a rotating, elliptical Earth excited by a double couple, *J. Phys. Earth,* **25,** 117–142, 1977.

Stein, S., and R.J. Geller, Time-domain observation and synthesis of split spheroidal and torsional free oscillations of the 1960 Chilean earthquake: Preliminary results, *Bull. Seismol. Soc. Amer.,* **68,** 325–332, 1978.

Stein, S., and J. A. Nunn, Analysis of split normal modes for the 1977 Indonesian earthquake, *Bull. Seismol. Soc. Am.,* **71,** 1031–1047, 1981.

Stein, S., and E. A. Okal, Speed and size of the Sumatra earthquake, *Nature,* **434,** 581–582, 2005.

Stein, S., and E. A. Okal, Ultra-long period seismic study of the December 2004 Indian Ocean earthquake and implications for regional tectonics and the subduction process, *Bull. Seismol. Soc. Am.,* **87,** S279–S295, 2007.

Synolakis, C.E., J.C. Borrero, H.M. Fritz, V.V. Titov, and E.A. Okal, Inundation during the 26

December 2004 tsunami, *Proc. 30th Intl. Conf. Coastal Eng.,* San Diego, in press, 2007.

Tolstoy, M., and D. B. Bohnenstiehl, Hydroacoustic constraints on the rupture duration, length, and speed of the great Sumatra-Andaman earthquake, *Seis. Res. Lett.,* **76,** 419, 2005.

Tsai, V. C., M. Nettles, G. Ekström, and A. M. Dziewonski, Multiple CMT source analysis of the 2004 Sumatra earthquake, *Geophys. Res. Lett.,* **32,** *(17),* L17304, doi:10.1029/2005GL023813, 4 pp., 2005.

Vigny, C., W. J. F. Simons, S. Abu, R. Bamphenyu, C. Satirapod, N. Choosakul, C. Subarya, A. Socquet, K. Omar, H. Z. Abidin, and B. A. C. Ambrosius, Insight into the 2004 Sumatra-Andaman earthquake from GPS measurements in Southeast Asia, *Nature,* **436,** 201–206, 2005.

Wessel, P., and W.H.F. Smith, Free software helps map and display data, *Eos, Trans. Amer. Geophys. Un.,* **72,** 441 and 445–446, 1991.

Widmer, R., G. Masters, and F. Gilbert, Observably-split multiplets – data analysis and interpretation in terms of large-scale aspherical structure, *Geophys. J. R. astron. Soc.,* **111,** 559–576, 1992.

Figure Captions

Figure 1.: Earthquakes with moments $M_0 \geq 3.5 \times 10^{28}$ dyn*cm recorded in the past 70 years. Note the absence of very large events between 1964 (Alaska) and 2004 (Sumatra). Moment estimates of the latter refer to the CMT catalog, and to values published by *Stein and Okal* [2005] (solid dot; *SO*) and *Tsai et al.* [2005] (open circle; *T*). *N* shows the reassessment of the 1964 Alaska source by *Nettles et al.* (2005). The stars on the horizontal axis illustrate progress in seismic instrumentation. Vertical labels similarly identify *Richter*'s [1935] introduction of the concept of magnitude, as well as milestones in information technology. The shaded band corresponds to the advent of plate tectonics.

Figure 2.: Spectrum of ${}_0S_3$ at Inuyama, Japan (INU). On this remarkable record, all seven singlets are resolvable ($m = +2$ only barely), and remarkably well fit using *Tsai et al.*'s [2005] composite source scaled to a full moment of 1.28×10^{30} dyn*cm (synthetic in red).

Figure 3.: Observation and modeling of the fundamental torsional mode, ${}_0T_2$. The synthetic spectra (in red) are computed using *Tsai et al.*'s [2005] composite source, scaled to the full moment listed in each frame.

Figure 4.: Observation and modeling of the ${}_2S_1$ spheroidal overtone at Black Forest Observatory (BFO). The synthetic spectra (in red) are computed using *Tsai et al.*'s [2005] composite source, scaled to the full moment listed above. Note the relatively poor fit of the $m = +1$ singlet. The energy at $f \approx 0.38$ mHz belongs to the torsional mode ${}_0T_2$.

Figure 5.: Splitting pattern of ${}_0S_2$ observed (black traces) and computed for a point source double-couple (red) at selected stations. Note that receivers located at comparable latitudes feature similar patterns, but that the latter vary strongly with latitude. All singlets are well recorded around 47°N (BFO, YSS), but the outer ones have already decreased sharply around 57°N (OBN, ARU), and only the central singlet ($m = 0$) is present at a sub-polar station (DRV; 67°S). By contrast, only the outer two singlets are visible at 38°N (MAJO, CMB), but all even ones ($m = 0, \pm 2$) are recorded in the equatorial band (NNA, KMB).

Figure 6.: Dependence of splitting pattern on source latitude. The left frames examine the evolution of the theoretical splitting patterns predicted at Obninsk (OBN) when a point source double-couple is moved north along the rupture area, as defined by the aftershock distribution (center). Note that the $m = \pm 1$ singlets are particularly sensitive to source latitude. Comparison with the observed multiplet (right) suggests a latitude of 7°N for the centroid of excitation, providing the best fit to this gravest oscillation by a point source double-couple. In particular, a rupture confined to the southern segment (shaded box on map), inferred in early source inversions, misfits the splitting pattern.

Figure 7.: Time-domain study of the outboard singlets ($m = \pm 3$) of ${}_0S_3$ at Matsushiro (MAJO). The exceptional quality of this 17–day record allows the isolation of singlets by directly narrow band-pass filtering the record, as sketched on the frequency domain records shown at left. For both singlets, the resulting time series is shown on the top frame, and its envelope, plotted in logarithmic units on the bottom one. Least-squares fitting of the latter by a straight line yields best-fitting Q (from the slope of the regression) and moment in dyn*cm (from its zero-intercept).

Figure 8.: Summary of moments obtained for each mode by best-fitting its spectra to that of a point-source double-couple. The square represents the CMT solution inverted at 300 s. *(a):* 2004 Sumatra earthquake; note the general increase of moment with period (regressed as the dashed line). *(b):* 2005 Nias earthquake. Note in this case the good agreement of modal fits to the CMT value inverted at shorter periods.

Figure 9.: *(a):* Results of *Tsai et al.*'s [2005] composite moment tensor inversion. The beachballs represent the focal mechanisms of the five components of the source, with their centroid time offset with respect to the initiation of rupture in bold, and their individual moments in bold italics. *(b):* The same procedure as on Figure 8*a* is used to best-fit the data to a source similar to *Tsai et al.*'s [2005], with only the total moment being free to vary. These results are essentially independent of frequency, and in excellent agreement with those authors' moment (dashed line).

Figure 10.: Time-domain measurement of the Q of ${}_0S_0$ from a stack of four high-quality 90–day

long time series. *(a):* Envelope of the time series of the mode obtained by combining a narrow-bandpass filtered stack with its Hilbert transform. The red line shows the best linear fit to the decay of the logarithm of the envelope with time, yielding $Q = 5579$. *(b):* Dependence of Q on the length of the window used for the regression. The window starts 5 days after the event and lasts from 10 to 80 days. Note the robustness of the result. The dashed line is the previously published value ($Q = 5700$). *(c):* Quality of fit as a function of value of Q, expressed as the ratio of the root-mean-square residual of the best linear fit to the decay of the envelope for an imposed Q, scaled to its value for the best-fitting Q. The red box illustrates the resulting one$-\sigma$ interval of confidence. The dashed line corresponds to $Q = 5700$.

Figure 11.: Comparison of time-domain regressions of the decay of ${}_0S_0$ at the same station (CTAO) for three recent earthquakes. *(a):* Same as Figure 5*a*, but for a single station. The envelope is plotted without deconvolution of the (common) instrument. Note the smoother data and superior fit for the 2004 Sumatra earthquake. *(b):* Same As Figure 10*b*, with Q values color-coded as on the top frame. Note that the measurement is robust only for the Sumatra earthquake.

Figure 12.: Investigation of the possible presence of ${}_2S_2$ in the BFO record. On all three frames, the black line is the observed ground motion spectrum and the red one shows the best fit to a point-source with the geometry of the Harvard CMT solution. In *(a)*, we synthesize only the high–Q mode ${}_3S_1$, in *(b),* we add the mantle mode ${}_1S_3$ and in finally in *(c)* we had the core mode ${}_2S_2$. In the latter case comparison with the synthetic *(b)*, reproduced in green, suggests that the contribution of ${}_2S_2$ remains on the order of the noise present in the sidelobes of the main modes.

TABLE 1. Best-fit moments measured in this study

Mode	Period (s)	Sumatra, 2004						Nias, 2005		
		Point Source			Composite Source			Point Source		
		Number of records	Best-fit moment (10^{29} dyn*cm)	*/	Number of records	Best-fit moment (10^{29} dyn*cm)	*/	Number of records	Best-fit moment (10^{29} dyn*cm)	*/
					Spheroidal and Radial Modes					
${}_0S_2$	3232	21	10.26	1.08	20	13.60	1.07			
${}_2S_1$	2476	5	11.21	1.30	5	9.88	1.11			
${}_0S_3$	2134	37	9.13	1.09	36	12.75	1.11	3	1.90	1.07
${}_0S_4$	1545	40	8.68	1.18	39	12.55	1.14	8	1.18	1.07
${}_1S_2$	1470	21	8.55	1.23	28	13.33	1.10			
${}_0S_0$	1227	40	7.79	1.07	40	11.57	1.09	2	1.45	1.05
${}_0S_5$	1190	41	9.07	1.25	33	13.45	1.15	8	1.41	1.10
${}_1S_3$ *	1062	40	7.62	1.15	40	11.34	1.13			
${}_0S_6$	964	46	9.87	1.35	22	14.38	1.10			
${}_3S_2$	903	15	6.39	1.19	14	9.64	1.15			
${}_1S_4$	852	21	6.74	1.22	19	12.15	1.15			
${}_1S_0$	613	42	5.96	1.16	42	13.71	1.17	10	1.28	1.15
					Torsional Modes					
${}_0T_2$	2632	2	10.24	1.69	2	12.92	1.07			
${}_0T_3$	1703	5	10.10	1.30	3	11.01	1.27			
${}_0T_4$	1304	11	8.30	1.44	9	11.08	1.28			
${}_0T_6$	925	13	8.21	1.31	18	11.46	1.22			
Average			**8.50**	**1.19**		**12.10**	**1.12**		**1.42**	**1.18**

* Includes ${}_3S_1$.

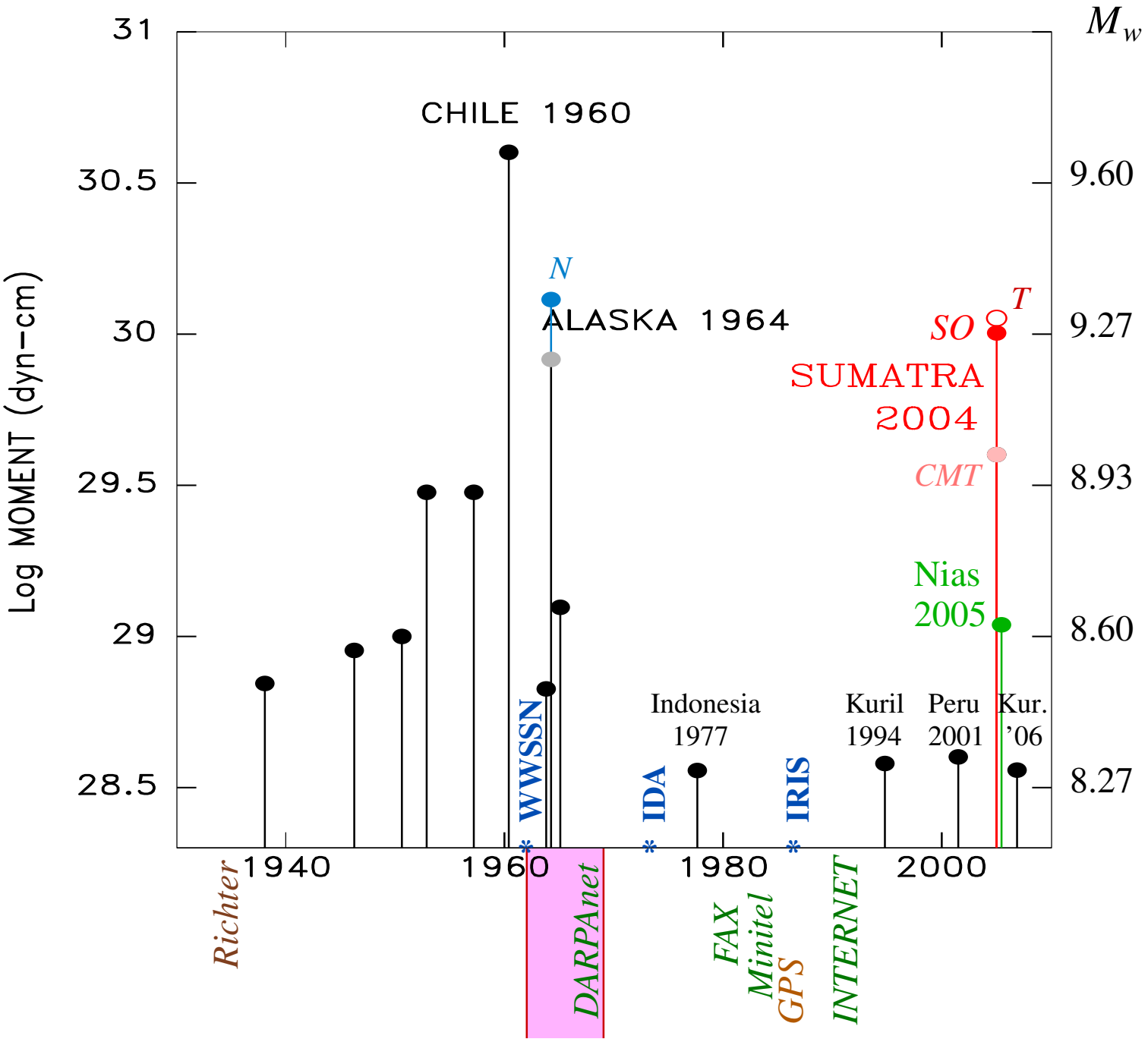
31
30.5
30
29.5
29
28.5
Log MOMENT (dyn−cm)
M_w
9.60
9.27
8.93
8.60
8.27
CHILE 1960
N
ALASKA 1964
T
SO
SUMATRA
2004
CMT
Nias
2005
Indonesia
1977
Kuril
1994
Peru
2001
Kur.
'06
WWSSN
IDA
IRIS
1940
1960
1980
2000
Richter
DARPAnet
FAX
Minitel
GPS
INTERNET

Figure 1

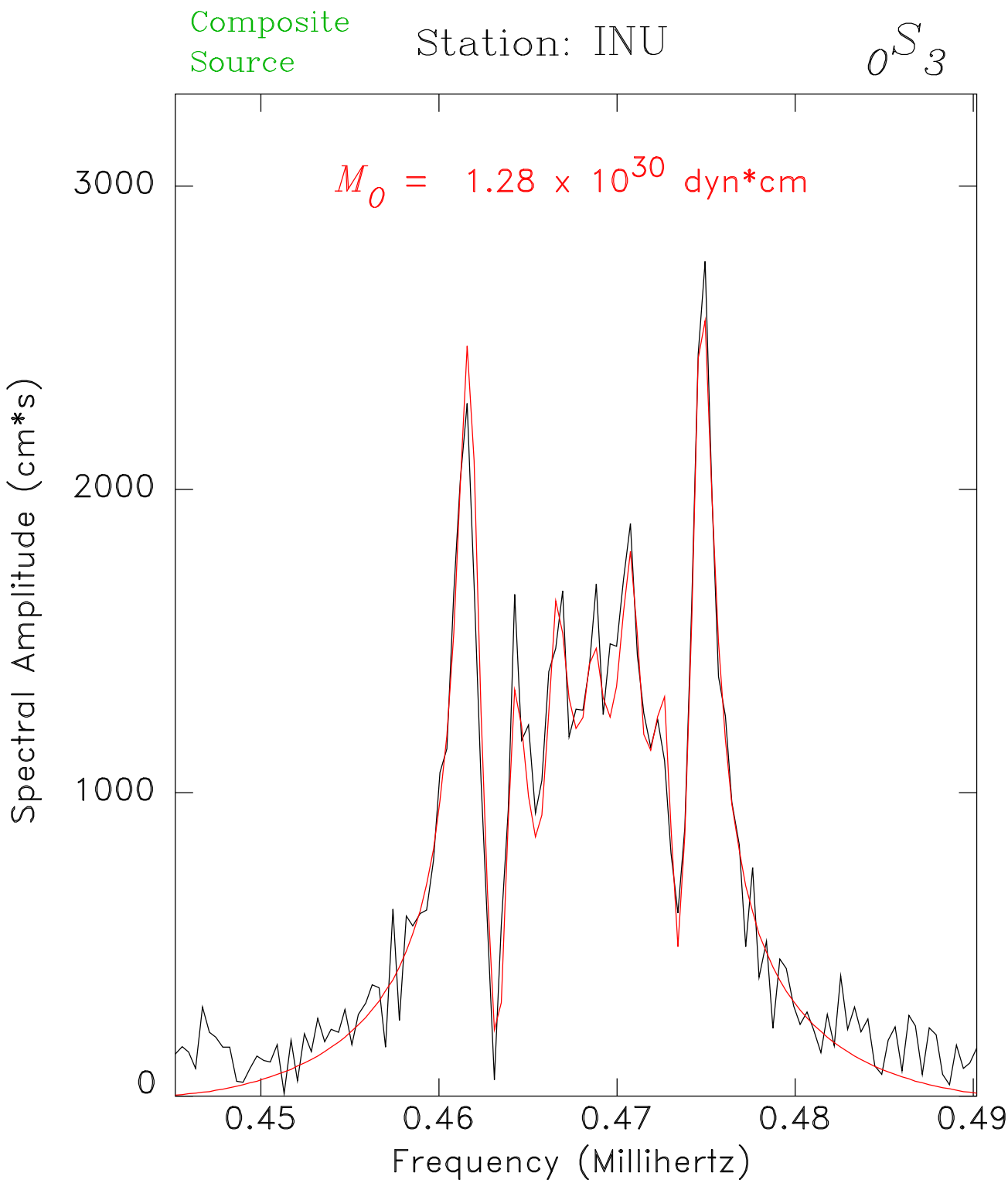
Composite
Source
Station: INU
$_0S_3$
M_0 = 1.28 x 10^{30} dyn*cm
3000
2000
1000
0
Spectral Amplitude (cm*s)
0.45
0.46
0.47
0.48
0.49
Frequency (Millihertz)

Figure 2

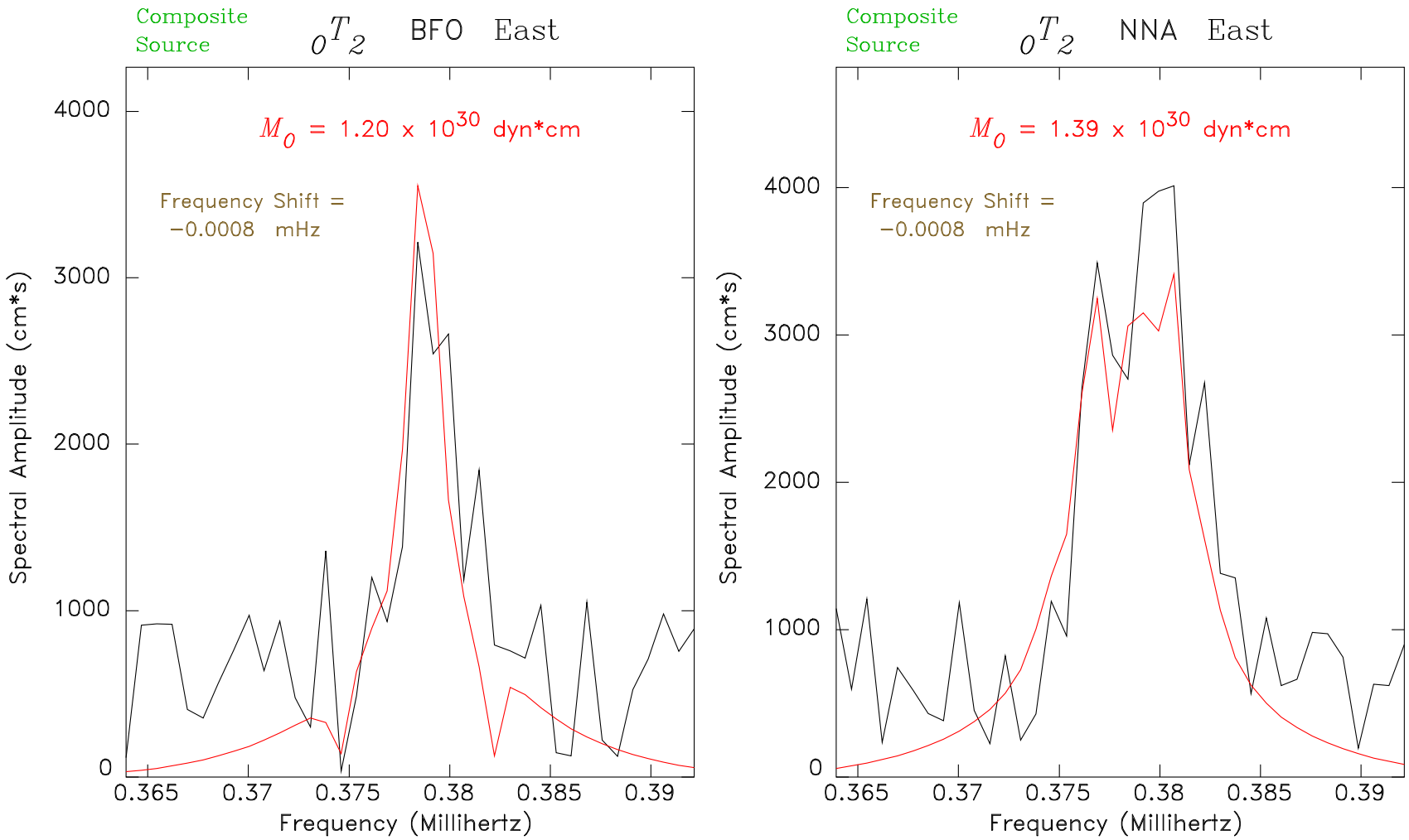
Composite Source
$_0T_2$ BFO East
M_0 = 1.20 x 10^{30} dyn*cm
Frequency Shift = −0.0008 mHz
Spectral Amplitude (cm*s)
Frequency (Millihertz)
Composite Source
$_0T_2$ NNA East
M_0 = 1.39 x 10^{30} dyn*cm
Frequency Shift = −0.0008 mHz
Spectral Amplitude (cm*s)
Frequency (Millihertz)

Figure 3

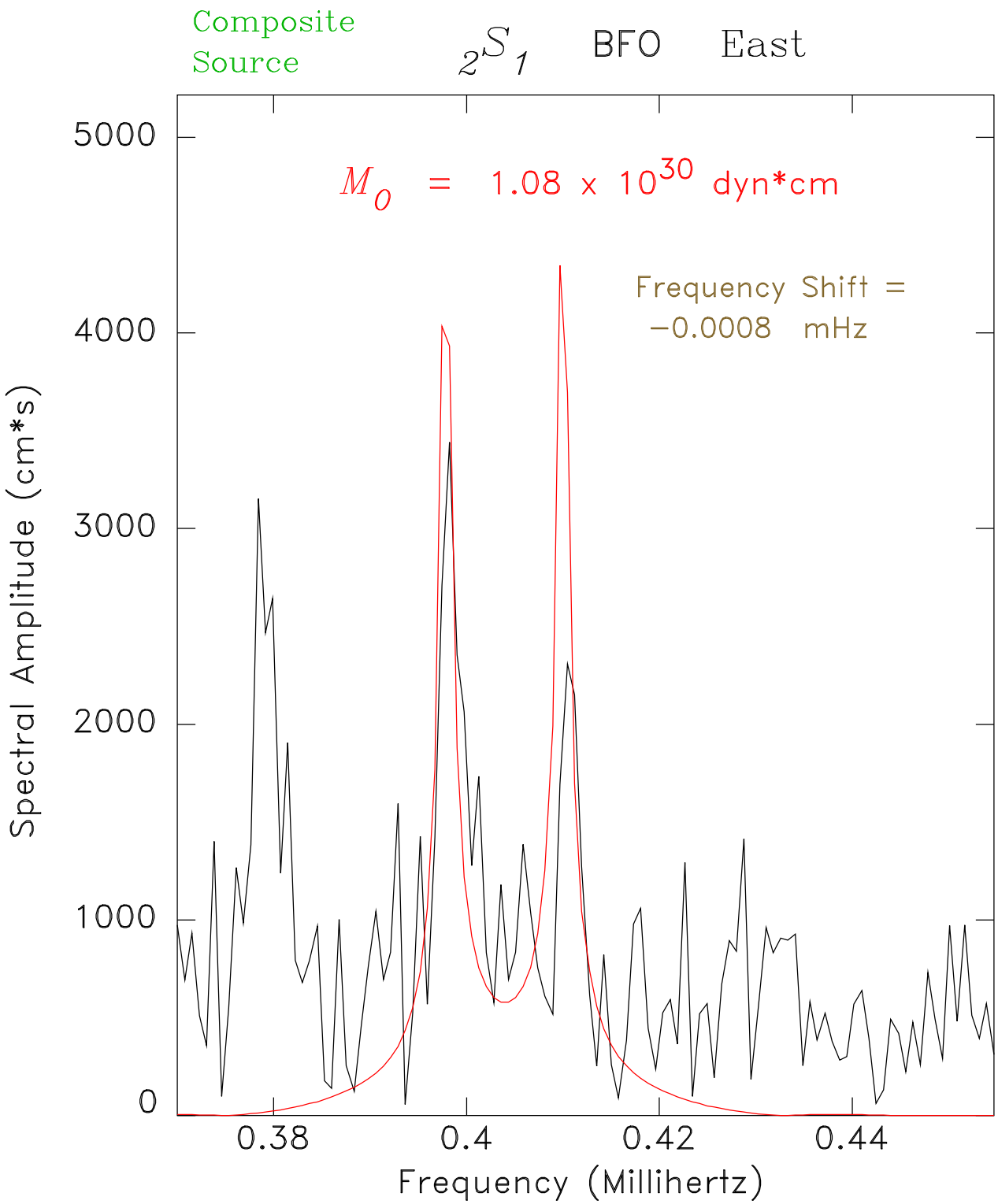
Composite
Source
$_2S_1$
BFO
East
M_0 = 1.08 x 10^{30} dyn*cm
Frequency Shift =
−0.0008 mHz
Spectral Amplitude (cm*s)
5000
4000
3000
2000
1000
0
0.38
0.4
0.42
0.44
Frequency (Millihertz)

Figure 4

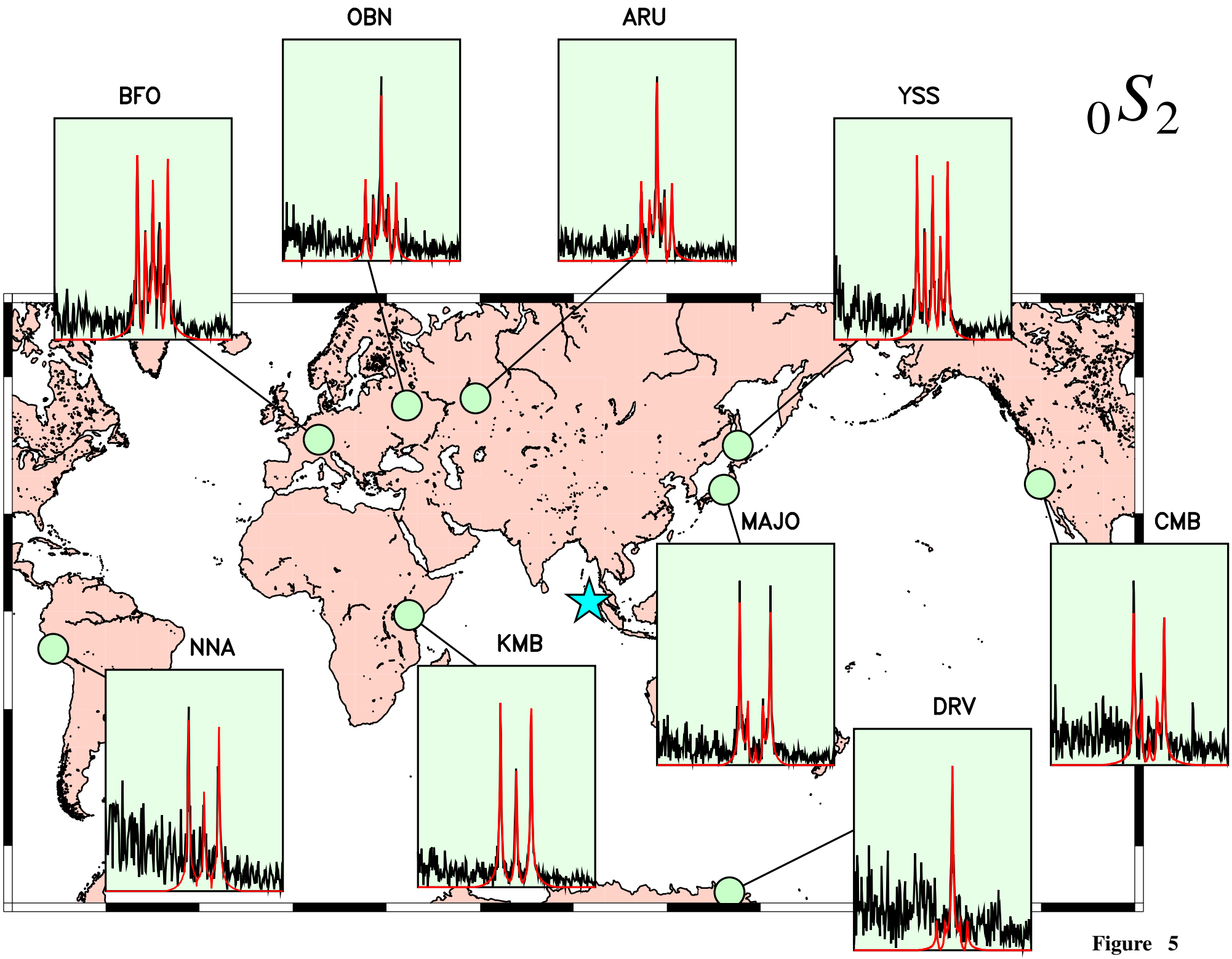

Figure 5

Splitting Patterns Constrain Source Centroid

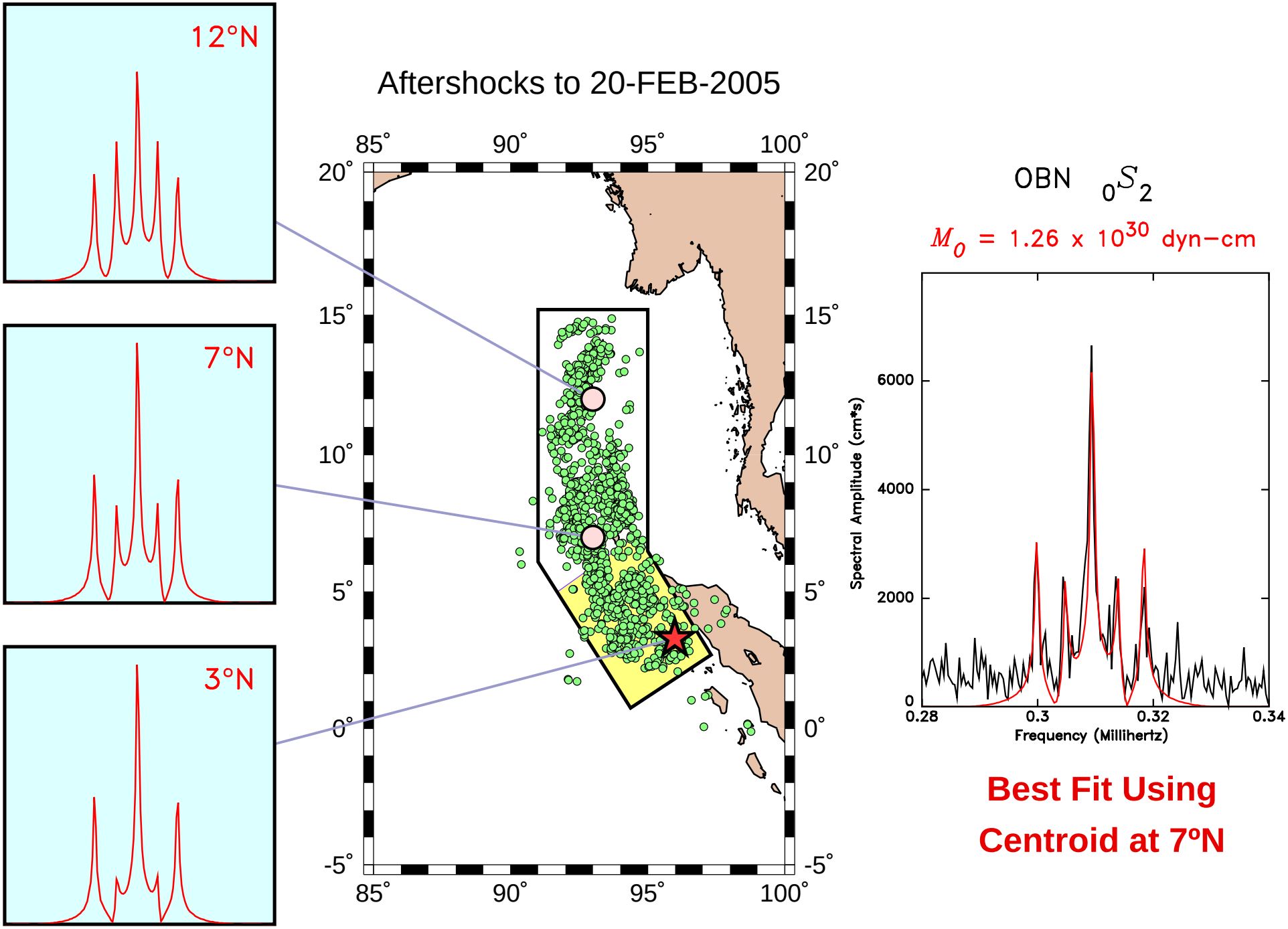

Figure 6

MAJO -- Matsushiro, Japan

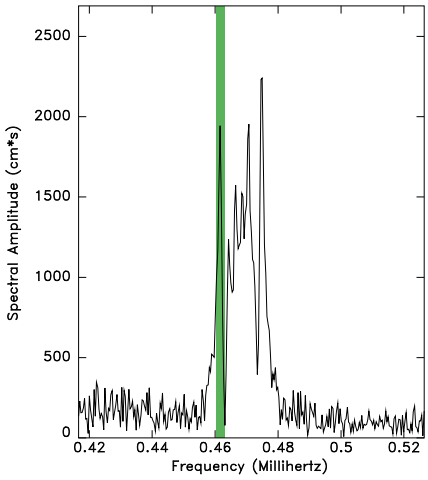

$_0S_3^{-3}$

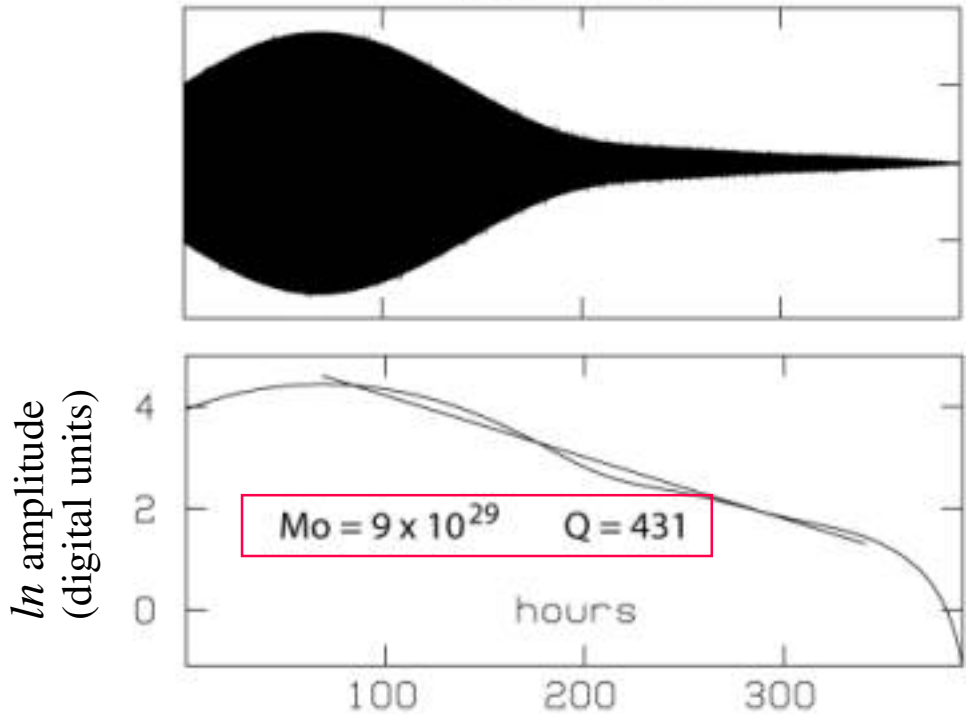

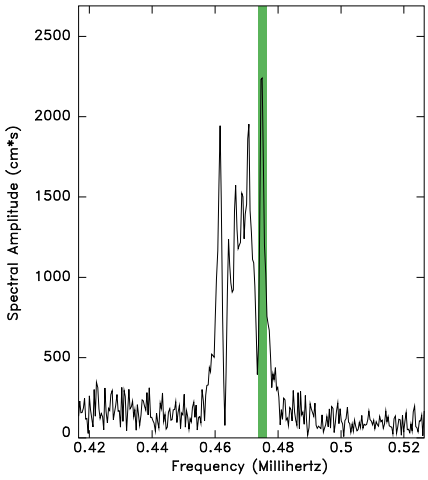

$_0S_3^{+3}$

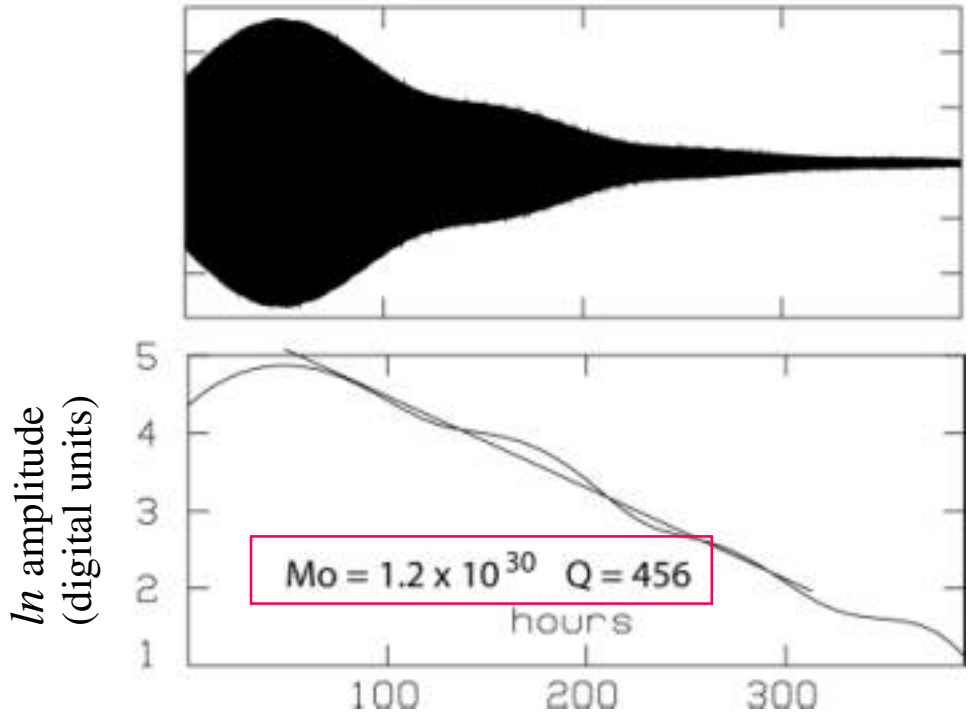

Figure 7

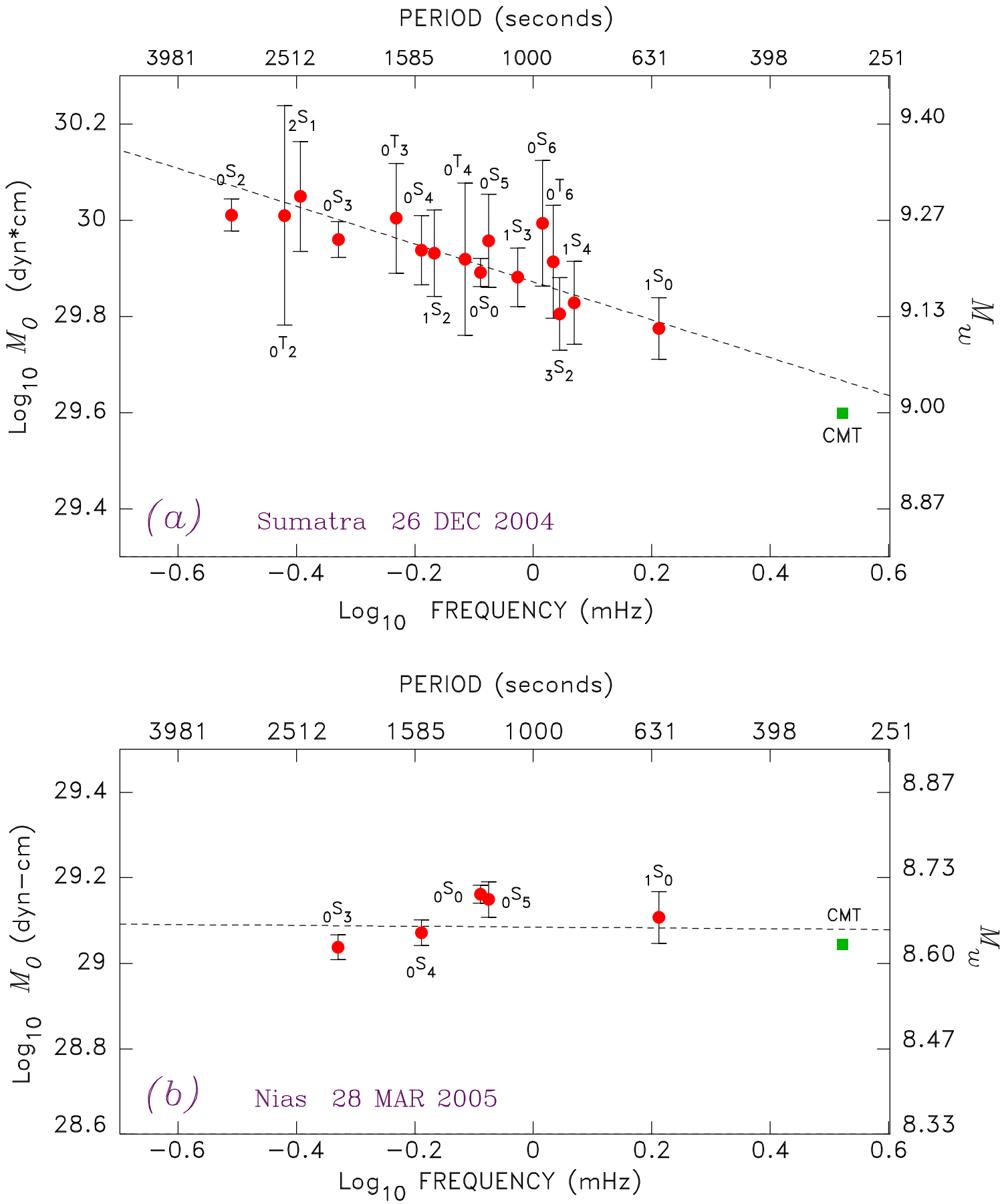
PERIOD (seconds)
3981
2512
1585
1000
631
398
251
30.2
30
29.8
29.6
29.4
Log10 M0 (dyn*cm)
9.40
9.27
9.13
9.00
8.87
Mw
0S2
2S1
0S3
0T3
0S4
0T4
0S5
0S6
0T6
1S3
1S4
1S0
1S2
0S0
0T2
3S2
CMT
(a)
Sumatra 26 DEC 2004
−0.6
−0.4
−0.2
0
0.2
0.4
0.6
Log10 FREQUENCY (mHz)
PERIOD (seconds)
3981
2512
1585
1000
631
398
251
29.4
29.2
29
28.8
28.6
Log10 M0 (dyn−cm)
8.87
8.73
8.60
8.47
8.33
Mw
0S3
0S0
0S5
1S0
0S4
CMT
(b)
Nias 28 MAR 2005
−0.6
−0.4
−0.2
0
0.2
0.4
0.6
Log10 FREQUENCY (mHz)

Figure 8

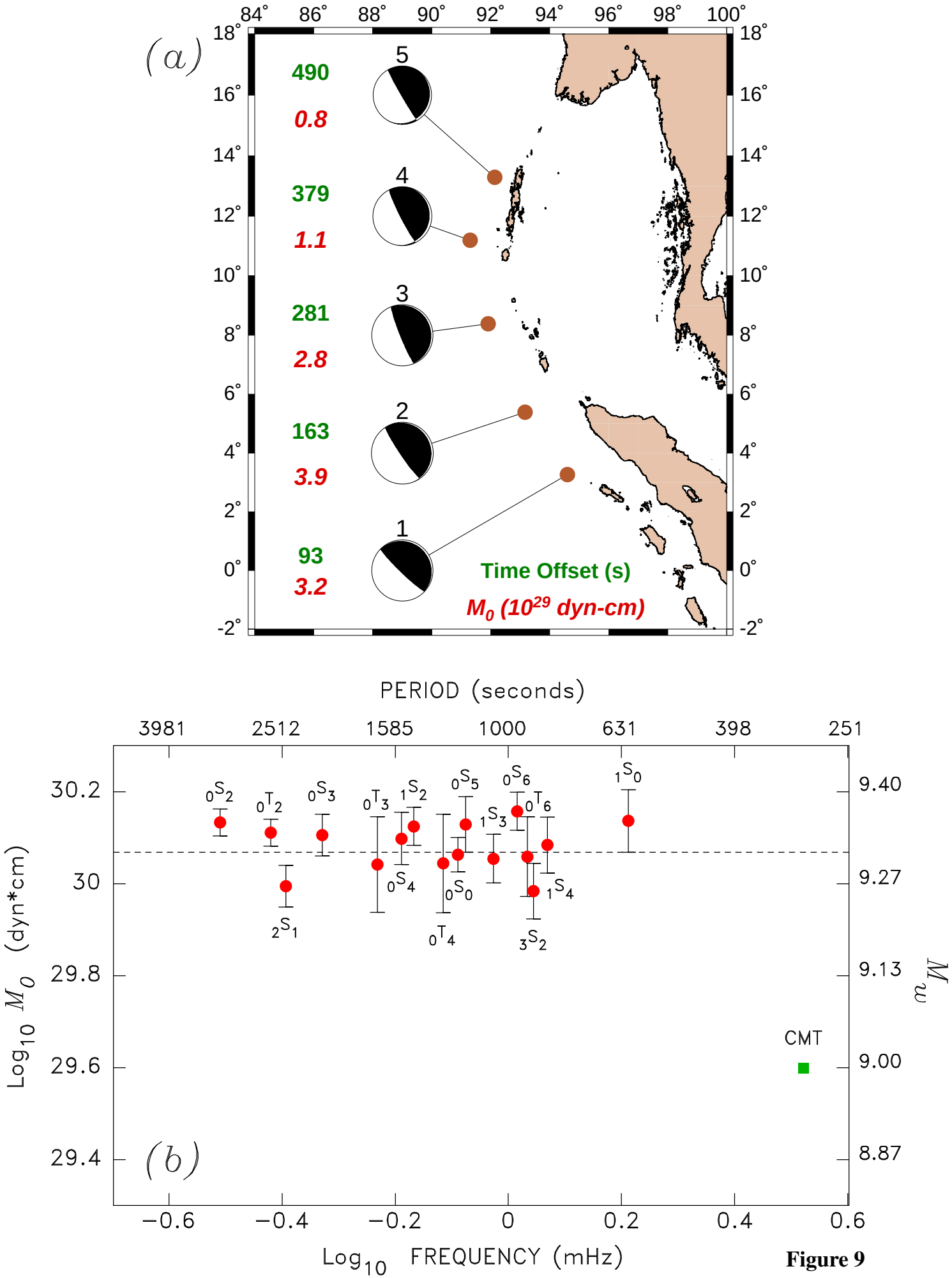
(a)
84° 86° 88° 90° 92° 94° 96° 98° 100°
18° 16° 14° 12° 10° 8° 6° 4° 2° 0° -2°
5
490
0.8
4
379
1.1
3
281
2.8
2
163
3.9
1
93
3.2
Time Offset (s)
M_0 (10^{29} dyn-cm)
PERIOD (seconds)
3981 2512 1585 1000 631 398 251
30.2 30 29.8 29.6 29.4
Log_{10} M_0 (dyn*cm)
9.40 9.27 9.13 9.00 8.87
M_w
$_0S_2$ $_0T_2$ $_0S_3$ $_0T_3$ $_1S_2$ $_0S_5$ $_0S_6$ $_1S_0$
$_1S_3$ $_0T_6$
$_0S_4$ $_0S_0$ $_1S_4$
$_2S_1$ $_0T_4$ $_3S_2$
CMT
(b)
−0.6 −0.4 −0.2 0 0.2 0.4 0.6
Log_{10} FREQUENCY (mHz)

Figure 9

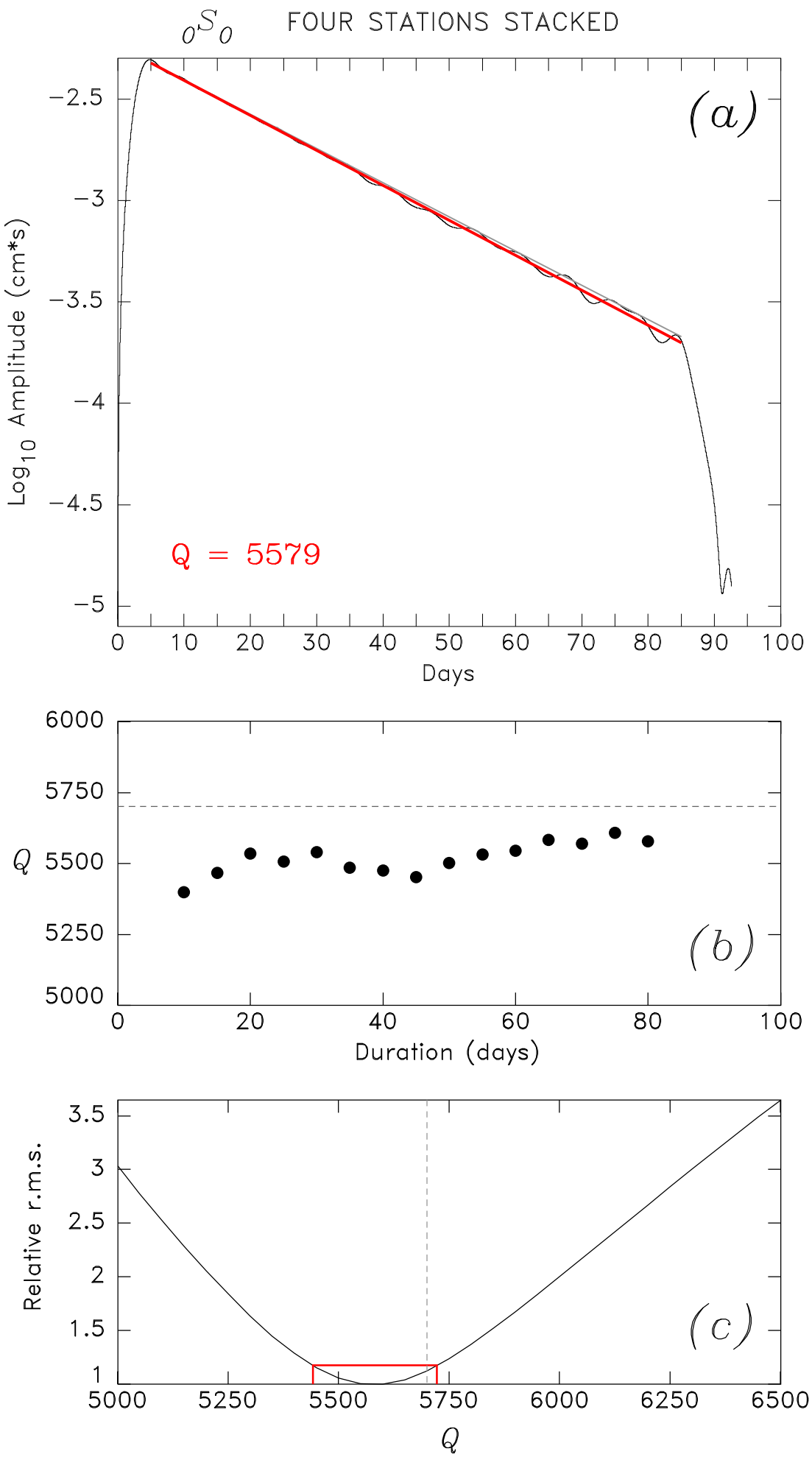
$_0S_0$ FOUR STATIONS STACKED
(a)
Log10 Amplitude (cm*s)
−2.5
−3
−3.5
−4
−4.5
−5
Q = 5579
0
10
20
30
40
50
60
70
80
90
100
Days
(b)
Q
6000
5750
5500
5250
5000
0
20
40
60
80
100
Duration (days)
(c)
Relative r.m.s.
3.5
3
2.5
2
1.5
1
5000
5250
5500
5750
6000
6250
6500
Q

Figure 10

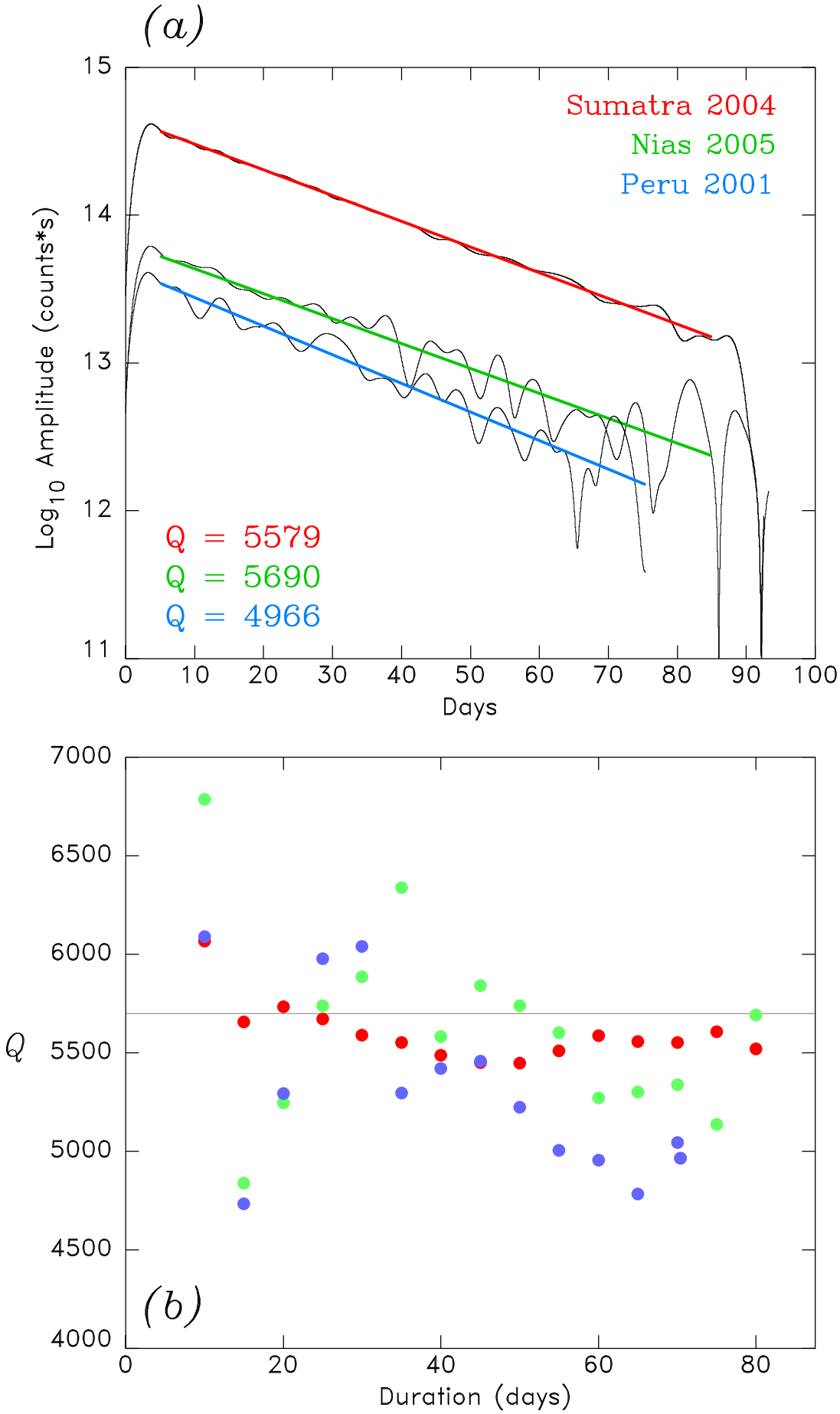
(a)
Sumatra 2004
Nias 2005
Peru 2001
Q = 5579
Q = 5690
Q = 4966
Log10 Amplitude (counts*s)
Days
(b)
Q
Duration (days)

Figure 11

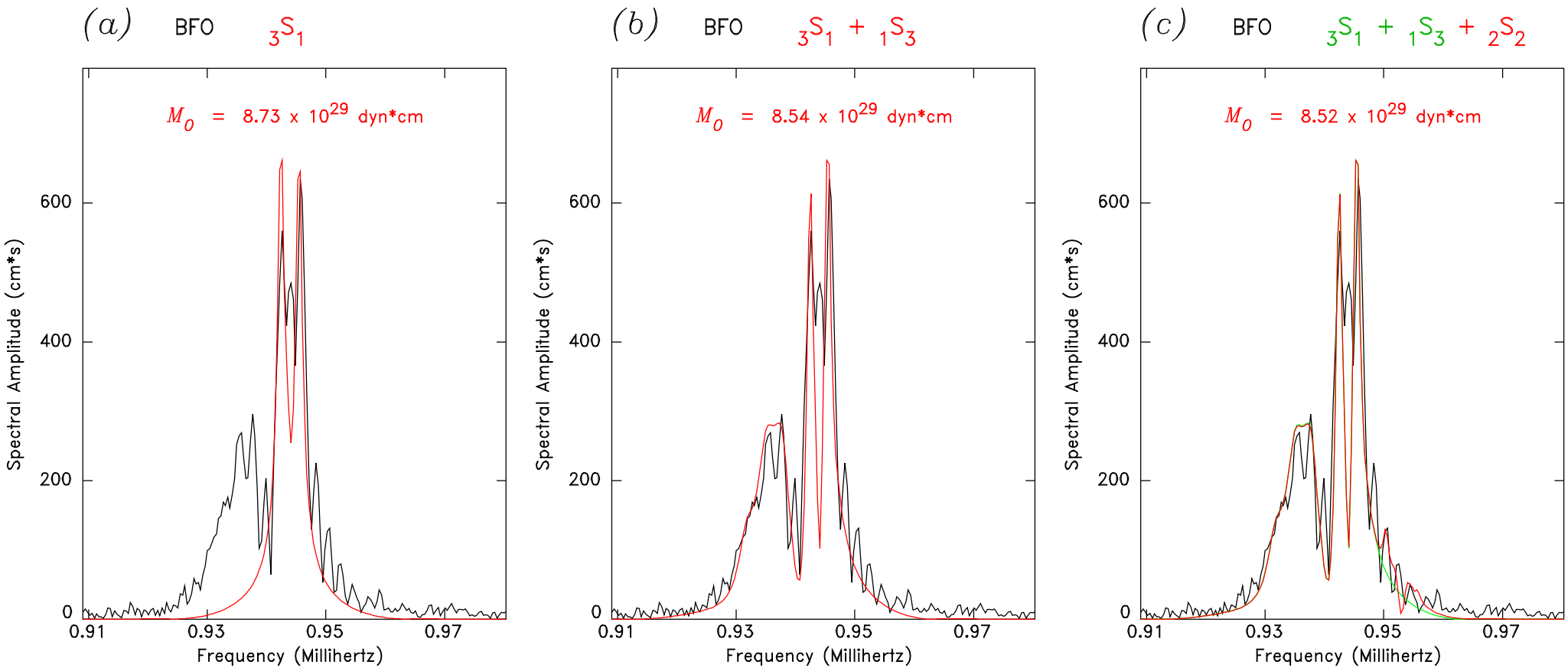
(a)
BFO
$_3S_1$
M_0 = 8.73 x 10^{29} dyn*cm
(b)
BFO
$_3S_1$ + $_1S_3$
M_0 = 8.54 x 10^{29} dyn*cm
(c)
BFO
$_3S_1$ + $_1S_3$ + $_2S_2$
M_0 = 8.52 x 10^{29} dyn*cm
Spectral Amplitude (cm*s)
0
200
400
600
0.91
0.93
0.95
0.97
Frequency (Millihertz)

Figure 12